Journal of the Optical Society of America B
OPTICAL PHYSICS

High-efficiency metasurface grating constituted by new Huygens particles with wide tuning ranges of transmission magnitudes and phases

YANG XU,[1,2] NIANXI XU,[1] HAI LIU,[1] DONGZHI SHAN,[1] NAITAO SONG,[1] AND JINSONG GAO[1,2,*]

[1]Key Laboratory of Optical System Advanced Manufacturing Technology, Changchun Institute of Optics, Fine Mechanics and Physics, Chinese Academy of Sciences, Changchun 130033, China
[2]University of the Chinese Academy of Sciences, Beijing 100049, China
*Corresponding author: nkxuyang@126.com

Received 16 March 2018; accepted 11 April 2018; posted 13 April 2018 (Doc. ID 326183); published 3 May 2018

A subwavelength-scale Huygens particle utilizing both electric and magnetic responses is proposed here. As the electric and magnetic responses of the proposed particle are independent of each other, arbitrary complex transmission coefficients covering all magnitudes from 0 to 0.9 and all phases (360°) can be achieved by varying its structural parameters. By properly engineering the distribution of transmission magnitudes and phases, a Huygens metasurface grating with excitation of +1 order harmonic is designed and fabricated. The measurement results are in agreement with the simulations, further demonstrating the validity of the designed Huygens particle and metasurface.

OCIS codes: (160.1245) Artificially engineered materials; (160.3918) Metamaterials.

https://doi.org/10.1364/JOSAB.35.001248

1. INTRODUCTION

As a two-dimensional equivalence of metamaterials, metasurfaces have strong abilities to perform wavefront control, such as beam bending [1–3], beam converging [4–6], and uniform scattering [7,8]. Different from conventional devices for wave transformations, e.g., lenses, prisms, and gratings, the thickness of metasurfaces can be negligible as compared to the wavelength in the surrounding medium, which positively contributes to the achievement of miniaturization and integration in practical application. Moreover, metasurfaces have lower loss and fewer fabrication challenges than metamaterials. Because of the aforementioned merits, metasurfaces have gained a lot of attention in recent years [9–17].

To fully and efficiently control electromagnetic (EM) wave propagation in practical applications, independent controls of magnitudes and phases are required. Yu *et al.* [18] first demonstrated that fascinating anomalous beams can be obtained by properly arranging V-shaped antennas with flexible abrupt phases. Although such metasurfaces could provide the function to achieve anomalous refraction and reflection, unnecessary ordinary beams are produced simultaneously, thus inevitably leading to low efficiencies in controlling EM waves. Working as a spatial filter, a frequency selective surface [19] (FSS) structure also could control both magnitude and phase conventionally. Recently, controlling the transmission phases by utilizing FSS structures has been extensively reported [20–23]. In order to obtain the full transmission phase, a multilayer cascaded FSS structure should be adopted. However, the thickness of this kind of cascaded structure is commonly too large compared with the wavelength in vacuum. To achieve high efficiency and low profile, a novel metasurface named the Huygens metasurface has been proposed, constructed using the Huygens particles [1]. In general, the Huygens metasurfaces proposed in papers [1] and [24] are complicated to implement, since they consist of many interspaced and stacked layers. For simplifying the fabrication, some new Huygens metasurfaces were designed and fabricated by photolithography on two bonded boards [25–27]. Nonetheless, the ranges of possible transmission coefficients of these Huygens particles are usually limited, which would further restrict the efficiency of the metasurface.

In this paper, we propose a high-efficiency and subwavelength-scale Huygens particle with a full coverage of transmission magnitudes and phases. As the electric and magnetic responses of the particle are independent of each other, the transmission magnitudes and phases can be controlled independently. Based on full-wave simulation results, arbitrarily complex transmission coefficients covering all transmission magnitudes from 0 to 0.9 and all possible phases (360°) are obtained. By properly choosing these Huygens particles with specific transmission coefficients, a Huygens metasurface grating with stimulation of only +1 order harmonic is designed

and fabricated. The measurement results of this prototype well coincide with numerical simulations, demonstrating the validity of the proposed particles and metasurface.

2. THEORY AND ANALYSIS

The schematic of a Huygens metasurface under the normal incidence is given in Fig. 1. For a predetermined field distribution in Region I, an arbitrary field at Region II can be produced by introducing fictitious electric and magnetic surface currents ($\vec{J}_s$ and $\vec{M}_s$) on the boundary. According to the boundary condition, the EM fields in such two regions satisfy the following equations:

$$\begin{aligned} \hat{e}_z \times (\vec{H}_2 - \vec{H}_1) &= \vec{J}_s \\ -\hat{e}_z \times (\vec{E}_2 - \vec{E}_1) &= \vec{M}_s, \end{aligned} \tag{1}$$

where $\vec{E}_1 = \vec{E}_i + \vec{E}_r$, $\vec{H}_1 = \vec{H}_i + \vec{H}_r$, and $\vec{E}_2 = \vec{E}_t$, $\vec{H}_2 = \vec{H}_t$ are the total fields in Regions I and II, respectively.

In the surface equivalence principle, only the tangential fields are required to specify the surface currents on the boundary. By taking the ratio of the surface currents to the averaged tangential fields on the boundary, the electric surface admittance ($\overline{\overline{Y}}_{\rm es}$) and magnetic surface impedance ($\overline{\overline{Z}}_{\rm ms}$) can be obtained [28]:

$$\begin{aligned} \vec{J}_s &= \overline{\overline{Y}}_{\rm es} \cdot \vec{E}_{t,{\rm av}|S} \\ \vec{M}_s &= \overline{\overline{Z}}_{\rm ms} \cdot \vec{H}_{t,{\rm av}|S}, \end{aligned} \tag{2}$$

in which the expressions $\vec{E}_{t,{\rm av}|S}$ and $\vec{H}_{t,{\rm av}|S}$ are the averaged tangential electric and magnetic fields on the surface, respectively. Here, the electric surface admittance and magnetic surface impedance are assumed to be isotropic ($Y_{\rm es}$ and $Z_{\rm ms}$), as the polarization of the incident wave is defined.

After the $Y_{\rm es}$ and $Z_{\rm ms}$ are determined by the EM field distributions, the Huygens metasurface is discretized into unit cells for realistic implementation. The $Y_{\rm es}$ and $Z_{\rm ms}$ of a given unit cell can be directly extracted from the complex reflection (R) and transmission (T) coefficients [29]:

$$\begin{aligned} Y_{\rm es} &= \frac{2}{\eta} \cdot \frac{1-(R+T)}{1+(R+T)} \\ Z_{\rm ms} &= 2\eta \cdot \frac{1+(R-T)}{1-(R-T)}, \end{aligned} \tag{3}$$

where η is the wave impedance of free space, $R = |S_{11}|e^{i\angle S_{11}}$, and $T = |S_{21}|e^{i\angle S_{21}}$. Since the Huygens metasurfaces are considered as lossless and passive, the normalized electric surface admittance and magnetic surface impedance ($Y_{\rm es}\eta$ and $Z_{\rm ms}/\eta$) must be purely imaginary. To fulfill this requirement, it can be shown that $|R \pm T| = 1$ from Eq. (3), which leads to

$$|S_{11}||S_{21}|\cos(\angle S_{11} - \angle S_{21}) = 0. \tag{4}$$

The achievable transmission and reflection coefficients with a passive and lossless metasurface can be revealed by the above equation. Admittedly, if transmission magnitude ($|S_{21}|$) is unity or zero, then transmission phase ($\angle S_{21}$) can take an arbitrary value. If $|S_{21}|$ is from zero to unity, then arbitrary $\angle S_{21}$ can still be obtained, but must satisfy $\angle S_{21} - \angle S_{11} = \pi/2 + m\pi$, $m = 0, 1$. By combining Eq. (3) with Eq. (4), the normalized electric surface admittance and magnetic surface impedance are achieved as follows:

$$\begin{aligned} Y_{\rm es}\eta &= -2j\tan\left(\frac{\angle S_{21} \mp \phi}{2}\right) \\ Z_{\rm ms}/\eta &= -2j\tan\left(\frac{\angle S_{21} \pm \phi}{2}\right), \end{aligned} \tag{5}$$

where $\varphi = \arctan(\sqrt{1-|S_{21}|^2}/|S_{21}|)$, and the upper and lower signs of $\mp$ in $Y_{\rm es}\eta$ and $\pm$ in $Z_{\rm ms}/\eta$ correspond to $m = 0, 1$ respectively.

According to Eq. (5) with $m = 0$, the normalized electric surface admittance and magnetic surface impedance required to produce certain transmission magnitude and phase is shown in Fig. 2. It is observed that an arbitrary transmission coefficient can be achieved, and its transmission magnitude and phase can be controlled independently with proper electric surface admittance and magnetic surface impedance. It is further indicated that the independent control of electric surface admittance and magnetic surface impedance is necessary for the arbitrary control of transmission magnitudes and phases.

As shown in Fig. 3, a subwavelength-scale Huygens particle is proposed, which consists of a horizontal symmetric anchor-shaped structure (SAS) and a vertical symmetrically connected split-ring resonator (SC-SRR), integrated on a F4B substrate ($\varepsilon_r = 2.65$, $\tan\delta = 0.009$). Note here that although our particle may be similar to some frequency selective structures in shape [30], the physical mechanisms of them are different. The frequency selective structures usually respond only to the electric field of an incident wave, while the Huygens particle is sensitive to both electric and magnetic fields of incident waves. As an electric dipole, the horizontal SAS in the middle layer mainly contributes the electric response. On the other hand, the magnetic response is primarily contributed by the vertical SC-SRR composed of connected metallic patterns in the top and bottom layers, which is serving as a magnetic dipole. As depicted in Fig. 3(a), the horizontal SAS is insensitive to the magnetic field for transverse electric (TE) polarization, since there are no metallic ring structures in the direction perpendicular to the magnetic field. Similarly, due to the existence of via, the patterns in the top and bottom layers are equipotential and the vertical SC-SRR would further have a weak response to the electric field for TE polarization. Apparently, by adjusting the size of horizontal SAS and vertical SC-SRR, independent controls of electric and magnetic responses can be realized.

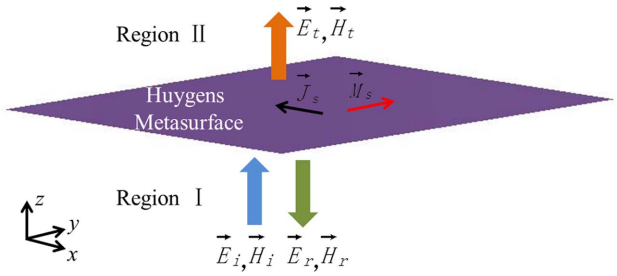

Fig. 1. Schematic of a Huygens metasurface under normal incidence of electromagnetic waves.

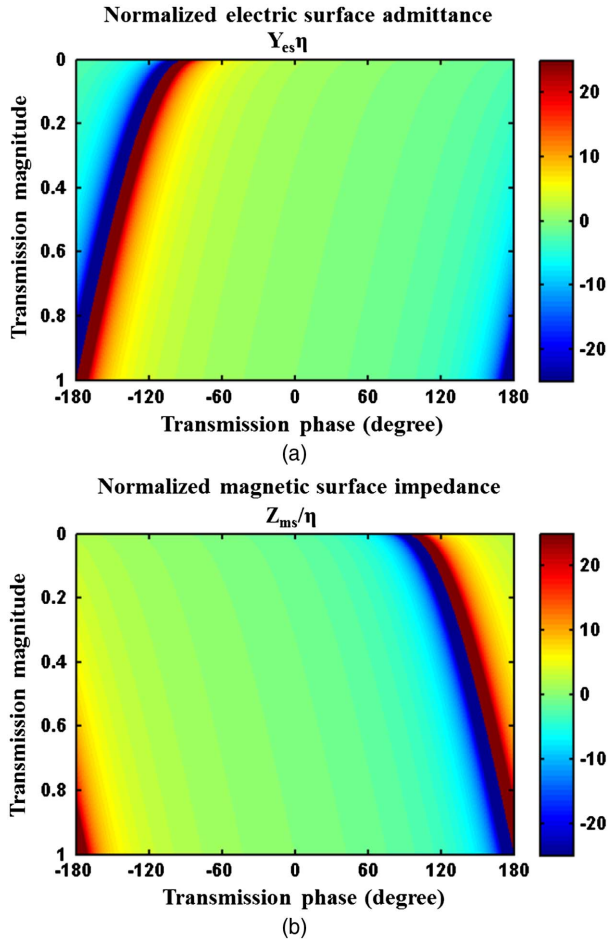

Fig. 2. Required normalized (a) electric surface admittance and (b) magnetic surface impedance with respect to the magnitude and phase of transmission.

To validate that, full-wave simulations of this particle are executed in the commercial software CST. In Fig. 4, the simulated values of $Y_{es}\eta$ and Z_{ms}/η at 6.7 GHz are given when scanning the geometrical parameters l_y and l. The other parameters of the Huygens particle are set as $p_x = 6.7$ mm, $p_y = 10$ mm, $t = 2$ mm, $l_1 = 4$ mm, $w = 0.4$ mm, $g = 0.2$ mm, $l_x = 1.4$ mm, and $s = 0.5$ mm. From Fig. 4(a), it can be observed that $Y_{es}\eta$ of the Huygens particle, characterizing the electrical response, is sensitive to the parameters l_y of horizontal SAS. Nevertheless, it is nearly unchanged at different values of parameters l of vertical SC-SRR. On the other hand, in Fig. 4(b), with the alteration of the parameters l of vertical SC-SRR, the Z_{ms}/η of the Huygens particle, characterizing the magnetic response, is changed obviously. However, it is almost invariable when the parameters l_y of horizontal SAS are swept. Therefore, the electric and magnetic responses of the proposed particle are independent of each other, and the coupling between them can be ignored.

In the procedures of designing the Huygens particle, the law that the electric response mainly relates to l_x and l_y and the magnetic response mainly relates to l is discovered. Hence, a database mapping transmission magnitude and phase to the values of l_x, l_y, and l is established with the help of CST.

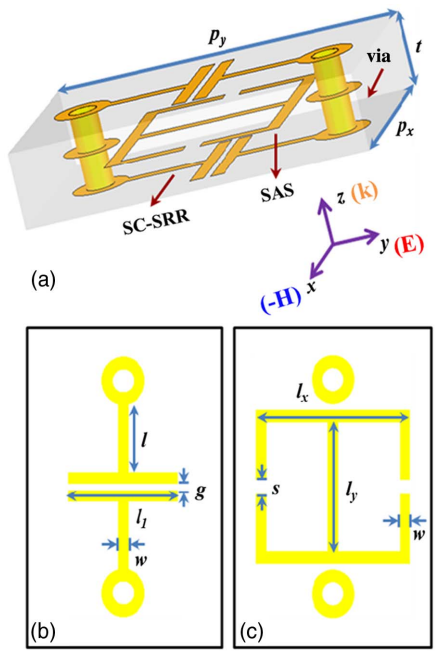

Fig. 3. Geometries of the proposed Huygens particle. (a) Side view. (b) Geometries of the top or bottom layer. (c) Geometries of the middle layer.

By extracting data from the database, we provide the transmission magnitude and phase of the Huygens particle at 6.7 GHz as functions of l_x, l_y, and l, which are depicted in Fig. 5. Note here, the values of l are discrete and not evenly spaced for clear observation. As shown in Fig. 5, full control of transmission magnitude ($0 \sim 1$) and phase ($-180° \sim 180°$) can be definitely achieved through changing the structural parameters of the proposed Huygens particle.

To clearly manifest the independent control of transmission magnitude and phase of our Huygens particle, the available range of transmission coefficients is displayed in Fig. 6(a) by extracting data (transmission magnitudes and phases) from Fig. 5. The orange area shows the available range, while the gray-blue area shows the unavailable range. Independent tuning of transmission magnitude and phase means that the arbitrary transmission phase from −180° to 180° can be achieved when the transmission magnitude is fixed to a certain value between 0 and 1, and vice versa. In other words, the realization of arbitrary complex transmission coefficients with modulus values from 0 to 1 would indicate that the transmission magnitude and phase are independent of each other. From Fig. 6(a), it can be observed that arbitrary complex transmission coefficients with modulus values from 0 to 0.9 can be obtained by using the Huygens particle we designed. Although our particle cannot fully cover the transmission magnitude from 0 to 1, its tuning range of transmission magnitude is already much higher than previous work [31]. The high transmission efficiency at 6.7 GHz is the result of the excitations of electric dipole resonance and magnetic dipole resonance at the same time. Figure 6(b) shows the corresponding surface currents in the Huygens particle for TE polarization, of which transmission magnitude and phase are 0.9 and 45° respectively. Evidently,

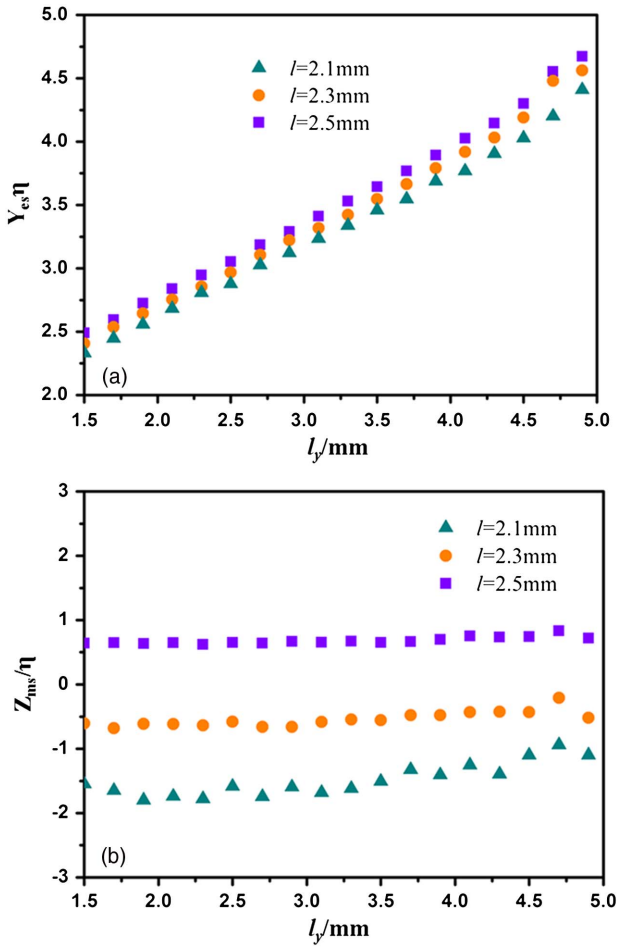

Fig. 4. Simulated (a) electric surface admittance and (b) magnetic surface impedance with respect to the variable parameters l_y and l.

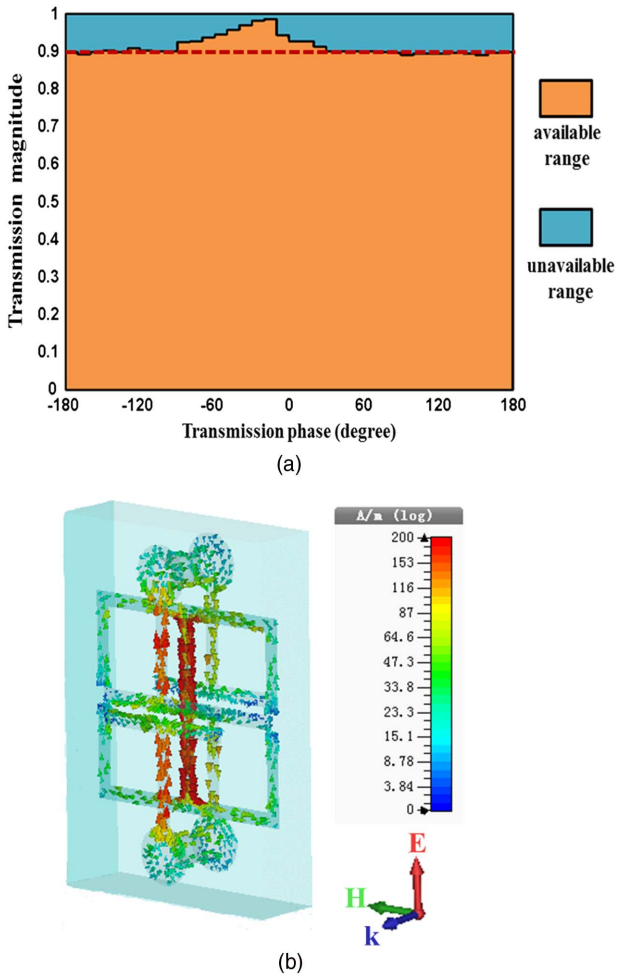

Fig. 6. (a) Available range of transmission magnitude and phase. (b) Surface current distribution of Huygens particle at 6.7 GHz with magnitude of 0.9 and phase of 45°.

the surface currents flowing from upper to lower parts of the SAS could mimic the radiation pattern of the electric dipole, and the circulating currents, which flow along the SC-SRR structure, would generate the magnetic dipole response. When designing functional metasurfaces, we can obtain different values of transmission coefficients by searching from the database for different parameters of the Huygens particles.

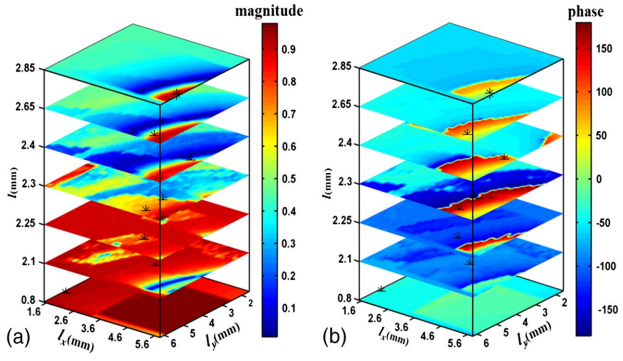

Fig. 5. Transmission (a) magnitude and (b) phase of Huygens particle at 6.7 GHz with respect to different structural parameters l_x, l_y, and l.

3. DESIGN AND EXPERIMENT

One Huygens metasurface grating that produces only +1 order diffraction is designed here by utilizing the proposed Huygens particles. To obtain the distributions of transmission magnitude and phase in the metasurface, the general expression of the transmission coefficient for the grating is adopted as follows:

$$t(x) = A(x)e^{j\phi(x)} = \sum_n A_n e^{-jn\frac{2\pi}{d}x}, \tag{6}$$

where d is the grating period, n is the diffraction order, and A_n is the magnitude of nth order diffraction. According to equation (6), the required transmission magnitudes and phases of the Huygens metasurface grating are denoted by solid lines in Fig. 7(a).

For this metasurface grating, we set eight particles in each period, and therefore the period is 53.6 mm. The symbols "■" in Fig. 7(a) show the designed values of transmission magnitude and phase corresponding to different particles. After searching from the database, the structural parameters of eight Huygens particles are determined and marked by "*" in Fig. 5. We further marked the simulated transmission magnitude and

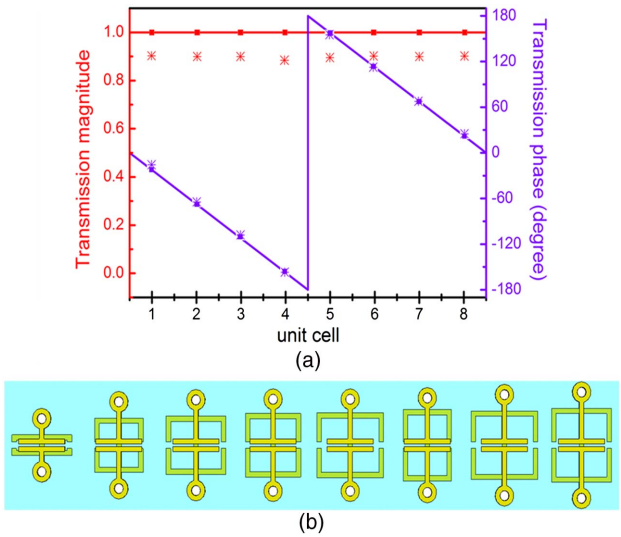

Fig. 7. (a) Transmission magnitude and phase profiles of the metasurface grating. (b) One period of the simulation model of the Huygens metasurface grating.

phase of these eight Huygens particles by "*" in Fig. 7(a), from which the simulated values of transmission magnitude and phase are basically consistent with the designed values, except the 10% decline of simulated transmission magnitudes. One period of the simulation model of the Huygens metasurface grating is depicted in Fig. 7(b). Based on the relation between refraction angle and the periodicity $p = \lambda/\sin(\phi)$ [32], this metasurface grating structure can achieve a 57° beam-refraction at 6.7 GHz with respect to normal incidence.

To verify the design of the metasurface grating, a full-wave simulation is performed in the CST Microwave Studio. Unit-cell boundaries and Floquet ports are applied in the simulation to imitate infinite metasurface structure. Figure 8(a) shows the simulated *S*-parameters of Floquet harmonics. It is observed that most of the incident power couples to the transmitted +1 harmonic, while the other harmonics are in the state of minimal excitation. The simulated Floquet harmonics prove that the desired +1 order diffraction is excited by this Huygens metasurface at around 6.7 GHz. The distribution of the electric field in Fig. 8(b) intuitively demonstrates that the plane wave normally incident from the bottom is steered to $\phi = 57°$ by the proposed metasurface grating. There are some slight fluctuations in the electric field distribution, which can be attributed to the excitation of other transmitted and reflected harmonics. The far-field characteristics of this metasurface grating are also investigated, and the normalized simulation results are depicted in Fig. 8(c). The far-field pattern shows that the main lobe points at the azimuth angle of –57° at 6.6 GHz, 6.7 GHz, 6.8 GHz, and 6.9 GHz, which implies that the proposed structure can perform in a relatively wide frequency band. The intensity of the main lobe is nearly 10 dB larger than the other side lobes at 6.6 GHz, 6.7 GHz, 6.8 GHz, and 6.9 GHz, verifying the high efficiency of the metasurface grating producing only +1 order diffraction.

The designed Huygens metasurface is fabricated by utilizing standard printed circuit board photographic and wet-etch

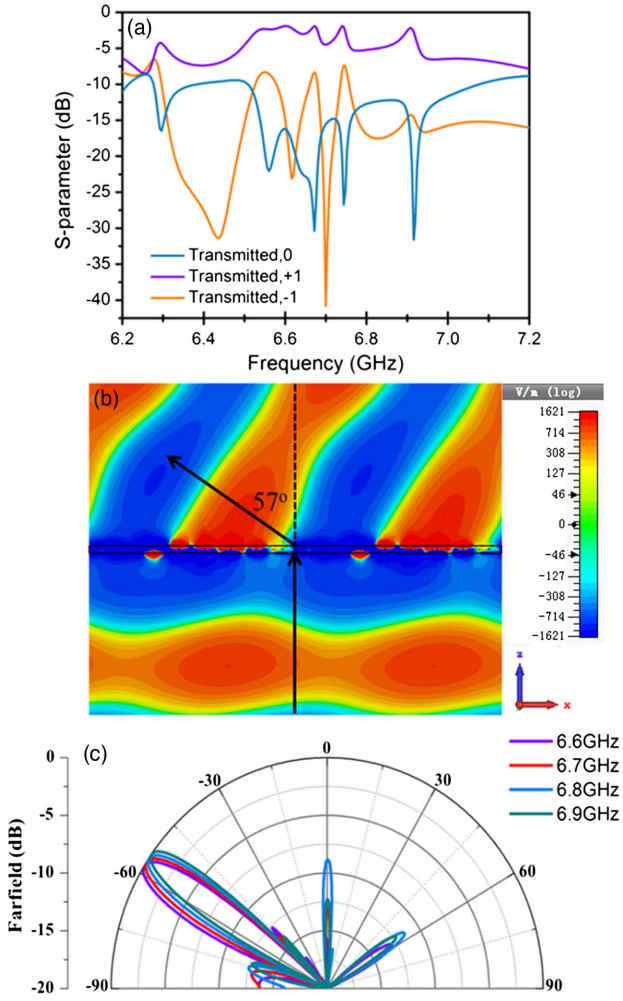

Fig. 8. Simulated results of the Huygens metasurface grating. (a) Simulated Floquet harmonics. (b) Simulated *y*-polarized electric fields at 6.7 GHz. (c) Normalized far-field patterns of the proposed metasurface grating.

techniques with a size of 300 mm × 300 mm, as shown in Fig. 9(a). To get a clearer view of the beam-refracting performance in a wide frequency band, a near-field measuring system is established, which is illustrated in Fig. 9(b). A lens antenna is selected as the source antenna in the experiment, as it can produce a Gaussian beam. In the location of the beam waist, where the prototype is placed, the EM wave is approximated as a quasi-plane wave. The lens antenna is connected to the transmitting port of an Agilent N5244A vector network analyzer. An open-ended, HD-70 waveguide probe is connected to the receive port, whose position can be controlled by a stepper motor. The near field over a 280 mm × 280 mm area is sampled every 7 mm × 7 mm. Then the far-field result is determined by appropriately Fourier transforming the measured near-field data. The measured far-field pattern of this Huygens metasurface is shown in Fig. 9(c). From the measurement results, we can learn that the operating frequencies of the proposed Huygens metasurface are higher than those in simulations, and there is a slight deviation for the main lobe compared with the simulation result. Besides that, more incident power is coupled to the

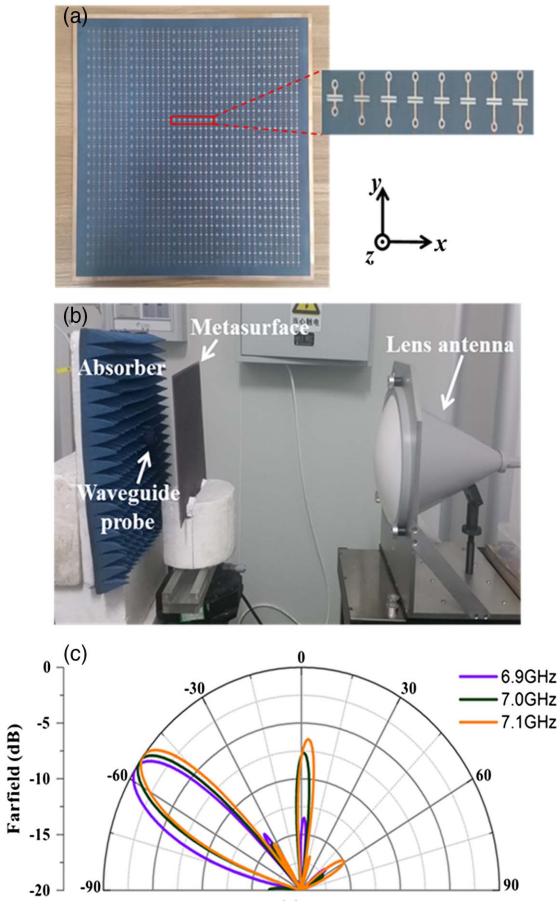

Fig. 9. Measured results of the Huygens metasurface grating. (a) Fabricated metasurface. Red rectangle shows one period of the metasurface. (b) Near-field measuring system. (c) Measured far-field pattern of the metasurface.

transmitted 0 order harmonic. These inconsistences are mainly caused by the non-strict plane-wave source generated by the lens antenna and fabrication tolerance of the prototype. Moreover, multiple reflections between the prototype and lens antenna would destroy the uniformity of the quasi-plane wave. Nevertheless, the intensity of main lobe is still 12.5 dB larger than the side lobes at 6.9 GHz, and therefore this experimental result positively demonstrates the validity of the Huygens metasurface we proposed.

4. CONCLUSION

In this paper, a Huygens particle composed of both electric and magnetic dipoles is realized. By adjusting its structural parameters, high efficiency and independent control of transmission magnitudes and phases can be achieved. Based on the Huygens particles, a Huygens metasurface grating with excitation of $+1$ order harmonic is designed and fabricated. An excellent match between the test and simulation results manifests that this metasurface can realize a good controlling performance in a relatively wide frequency band, which further proves the correctness of the proposed Huygens particle. In addition to beam deflection, this Huygens metasurface can also be applied in some fields such as computer-generated holography and low-side lobe antennas.

Funding. National Natural Science Foundation of China (NSFC) (11604329, 61401424).

REFERENCES

1. C. Pfeiffer and A. Grbic, "Metamaterial Huygens' surfaces: tailoring wave fronts with reflectionless sheets," Phys. Rev. Lett. **110**, 197401 (2013).
2. M. Selvanayagam and G. V. Eleftheriades, "Discontinuous electromagnetic fields using orthogonal electric and magnetic currents for wavefront manipulation," Opt. Express **21**, 14409–14429 (2013).
3. G. Silveira, L. Gabrielli, C. Hasnain, and H. Figueroa, "Breakthroughs in photonics 2013: advances in nanoantennas," IEEE Photon. J. **6**, 0700706 (2014).
4. F. Monticone, N. M. Estakhri, and A. Alu, "Full control of nanoscale optical transmission with a composite metascreen," Phys. Rev. Lett. **110**, 203903 (2013).
5. N. Kundtz and D. R. Smith, "Extreme-angle broadband metamaterial lens," Nat. Mater. **9**, 129–132 (2010).
6. F. Aieta, P. Genevet, M. A. Kats, N. Yu, R. Blanchard, Z. Gaburro, and F. Capasso, "Aberration-free ultrathin flat lenses and axicons at telecom wavelengths based on plasmonic metasurfaces," Nano Lett. **12**, 4932–4936 (2012).
7. T. J. Cui, M. Q. Qi, X. Wan, J. Zhao, and Q. Cheng, "Coding metamaterials, digital metamaterials and programmable metamaterials," Light Sci. Appl. **3**, e218 (2014).
8. K. Wang, J. Zhao, Q. Cheng, D. S. Dong, and T. J. Cui, "Broadband and broad-angle low-scattering metasurface based on hybrid optimization algorithm," Sci. Rep. **4**, 5935 (2014).
9. M. X. Ren, W. Wu, W. Cai, B. Pi, X. Z. Zhang, and J. J. Xu, "Reconfigurable metasurfaces that enable light polarization control by light," Light Sci. Appl. **6**, e16254 (2017).
10. T. J. Cui, S. Liu, and L. L. Li, "Information entropy of coding metasurface," Light Sci. Appl. **5**, e16172 (2016).
11. B. Memarzadeh and H. Mosallaei, "Array of planar plasmonic scatterers functioning as light concentrator," Opt. Lett. **36**, 2569–2571 (2011).
12. M. Papaioannou, E. Plum, J. Valente, E. T. Rogers, and N. I. Zheludev, "Two-dimensional control of light with light on metasurfaces," Light Sci. Appl. **5**, e16070 (2016).
13. L. H. Gao, Q. Cheng, J. Yang, S. J. Ma, J. Zhao, S. Liu, H. B. Chen, Q. He, W. X. Jiang, H. F. Ma, Q. Y. Wen, L. J. Liang, B. B. Jin, W. W. Liu, L. Zhou, J. Q. Yao, P. H. Wu, and T. J. Cui, "Broadband diffusion of terahertz waves by multi-bit coding metasurfaces," Light Sci. Appl. **4**, e324 (2015).
14. K. Chen, Y. Feng, F. Monticone, J. Zhao, B. Zhu, T. Jiang, L. Zhang, Y. Kim, X. Ding, S. Zhang, A. Alù, and C. W. Qiu, "A reconfigurable active Huygens' metalens," Adv. Mater. **29**, 1606422 (2017).
15. X. Ding, F. Monticone, K. Zhang, L. Zhang, D. Gao, S. N. Burokur, A. de Lustrac, Q. Wu, C. W. Qiu, and A. Alù, "Ultrathin pancharatnam-berry metasurface with maximal cross-polarization efficiency," Adv. Mater. **27**, 1195–1200 (2015).
16. F. Qin, L. Ding, L. Zhang, F. Monticone, C. C. Chum, J. Deng, S. Mei, Y. Li, J. Teng, M. Hong, S. Zhang, A. Alù, and C. W. Qiu, "Hybrid bilayer plasmonic metasurface efficiently manipulates visible light," Sci. Adv. **2**, e1501168 (2016).
17. L. Zhang, S. Mei, K. Huang, and C. W. Qiu, "Advances in full control of electromagnetic waves with metasurfaces," Adv. Opt. Mater. **4**, 818–833 (2016).
18. N. Yu, P. Genevet, M. A. Kats, F. Aieta, J. P. Tetienne, F. Capasso, and Z. Gaburro, "Light propagation with phase discontinuities: generalized laws of reflection and refraction," Science **334**, 333–337 (2011).
19. B. A. Munk, *Frequency-Selective Surfaces: Theory and Design* (Wiley, 2000).

20. A. H. Abdelrahman, A. Z. Elsherbeni, and F. Yang, "Transmission phase limit of multilayer frequency-selective surfaces for transmitarray designs," IEEE Trans. Antenna Propag. **62**, 690–697 (2014).
21. C. G. M. Ryan, M. R. J. Shaker, J. R. Bray, Y. M. M. Antar, and A. Ittipiboon, "A wideband transmitarray using dual-resonant double square rings," IEEE Trans. Antenna Propag. **58**, 1486–1493 (2010).
22. C. Pfeiffer and A. Grbic, "Millimeter-wave transmitarrays for wavefront and polarization control," IEEE Trans. Microw. Theory Tech. **61**, 4407–4417 (2013).
23. C. Pfeiffer, N. K. Emani, A. M. Shaltout, A. Boltasseva, V. M. Shalaev, and A. Grbic, "Efficient light bending with isotropic metamaterial Huygens' surfaces," Nano Lett. **14**, 2491–2497 (2014).
24. Y. Wang, Y. Liu, C. Liu, B. Sun, X. Sun, F. Li, and Y. Lu, "New design for transmitted phase of reflectionless metasurfaces with 2π coverage," IEEE Photon. J. **7**, 2701108 (2015).
25. S. L. Jia, X. Wan, D. Bao, Y. J. Zhao, and T. J. Cui, "Independent controls of orthogonally polarized transmitted waves using a Huygens metasurface," Laser Photon. Rev. **9**, 545–553 (2015).
26. J. P. S. Wong, M. Selvanayagam, and G. V. Eleftheriades, "Design of unit cells and demonstration of methods for synthesizing Huygens metasurfaces," Photon. Nanostr. **12**, 360–375 (2014).
27. S. L. Jia, X. Wan, X. J. Fu, Y. J. Zhao, and T. J. Cui, "Low-reflection beam refractions by ultrathin Huygens metasurface," AIP Adv. **5**, 067102 (2015).
28. E. F. Kuester, M. A. Mohamed, M. P. May, and C. L. Holloway, "Averaged transition conditions for electromagnetic fields at a metafilm," IEEE Trans. Antenna Propag. **51**, 2641–2651 (2003).
29. C. L. Holloway, M. A. Mohamed, E. F. Kuester, and A. Dienstfrey, "Reflection and transmission properties of a metafilm: with an application to a controllable surface composed of resonant particles," IEEE Trans. Electromagn. Compat. **47**, 853–865 (2005).
30. A. K. Rashid, B. Li, and Z. Shen, "An overview of three-dimensional frequency-selective structures," IEEE Antennas Propag. Mag. **56**, 43–67 (2014).
31. M. Kim, A. M. H. Wong, and G. V. Eleftheriades, "Optical Huygens' metasurfaces with independent control of the magnitude and phase of the local reflection coefficients," Phys. Rev. X **4**, 041042 (2014).
32. H. T. Chen, A. J. Taylor, and N. Yu, "A review of metasurfaces: physics and applications," Rep. Prog. Phys. **79**, 076401 (2016).